




## Article

# Synthesis of Novel Luminescent Double-Decker Silsesquioxanes Based on Partially Condensed TetraSilanolPhenyl POSS and Tb<sup>3+</sup>/Eu<sup>3+</sup> Lanthanide Ions

Stefano Marchesi <sup>1</sup>, Chiara Bisio <sup>1,2,\*</sup> and Fabio Carniato <sup>1,\*</sup>

<sup>1</sup> Dipartimento di Scienze e Innovazione Tecnologica, Università degli Studi del Piemonte Orientale “Amedeo Avogadro”, 15121 Alessandria, Italy; stefano.marchesi@uniupo.it

<sup>2</sup> CNR-SCITEC Istituto di Scienze e Tecnologie Chimiche “G. Natta”, Via C. Golgi 19, 20133 Milano, Italy

\* Correspondence: chiara.bisio@uniupo.it (C.B.); fabio.carniato@uniupo.it (F.C.); Tel.: +39-013-136-0216 (C.B.); +39-013-136-0217 (F.C.)

**Abstract:** In this study, novel lanthanide-containing double-decker polyhedral oligomeric silsesquioxanes (POSS) were prepared by combining the partially condensed TetraSilanolPhenyl POSS with terbium (Tb<sup>3+</sup>) and europium (Eu<sup>3+</sup>) ions. This open-cage POSS possesses four diametrically opposite silanol groups that are able to coordinate, under mild conditions, different luminescent ions through a simple corner-capping method. The two metal-containing POSS functionalized with Tb<sup>3+</sup> and with an equimolar combination of Tb<sup>3+</sup> and Eu<sup>3+</sup> show a completely condensed structure with different luminescent properties. Their emission features depend on the chemical nature of the metal ions incorporated in the framework. An improved Stokes shift was detected in the bimetallic compound containing both the Tb<sup>3+</sup> and Eu<sup>3+</sup> ions, promoted by the occurrence of a Tb<sup>3+</sup> → Eu<sup>3+</sup> energy transfer mechanism. These characteristics identify this metal-functionalized silica platform as a potential candidate for the development of novel luminescent devices.

**Keywords:** silsesquioxane; double-decker silsesquioxane; POSS; metal-functionalized POSS; corner-capping; lanthanide; europium; terbium; luminescence; energy transfer



**Citation:** Marchesi, S.; Bisio, C.; Carniato, F. Synthesis of Novel Luminescent Double-Decker Silsesquioxanes Based on Partially Condensed TetraSilanolPhenyl POSS and Tb<sup>3+</sup>/Eu<sup>3+</sup> Lanthanide Ions.

*Processes* **2022**, *10*, 758.

<https://doi.org/10.3390/pr10040758>

Academic Editor: Kang Hyun Park

Received: 21 March 2022

Accepted: 11 April 2022

Published: 13 April 2022

**Publisher’s Note:** MDPI stays neutral with regard to jurisdictional claims in published maps and institutional affiliations.



**Copyright:** © 2022 by the authors. Licensee MDPI, Basel, Switzerland. This article is an open access article distributed under the terms and conditions of the Creative Commons Attribution (CC BY) license (<https://creativecommons.org/licenses/by/4.0/>).

## 1. Introduction

Metal-containing polyhedral oligomeric silsesquioxanes (M-POSS) [1–6] are an important class of inorganic compounds consisting of a condensed oligomeric silica structure with a typical cage shape and bearing a metal ion in one vertex of the structure [7,8]. The remaining edges of the cage are occupied by silicon atoms that are covalently bonded to oxygen and to organic arms, thus generating a three-dimensional Si-O-Si skeleton with tetrahedral units ((RSiO<sub>1.5</sub>)<sub>n</sub>) (n = 4, 6, 8, 10, 12; R = H or organic substituents) [9–13]. In addition to fully condensed POSS, which is commonly identified by a R<sub>8</sub>Si<sub>8</sub>O<sub>12</sub> cubic structure [9–12], the most common cage-like silsesquioxanes used for the synthesis of M-POSS are the partially condensed TriSilanol POSS with the R<sub>7</sub>Si<sub>7</sub>O<sub>9</sub>(OH)<sub>3</sub> molecular formula [14–16]. The latter shows a siloxane structure containing three reactive silanol groups that are able to coordinate a broad spectrum of metal centres through a corner-capping procedure [12,17]. Following this synthetic approach, the metal ions are directly incorporated within the POSS inorganic core [6,12,17]. Another interesting strategy for the preparation of M-POSS is based on the chelation of the metal precursors, which is promoted by the presence of ligand arms attached to the silicon vertices [18–20].

POSS and their metal-functionalized derivatives typically exhibit molecular sizes, high chemical versatility and good mechanical and thermal stabilities [8,21]. Furthermore, these solids attracted an increasing interest in several scientific and technological fields, finding applications as heterogeneous catalysts [5,6,22,23] for biomedical and diagnostic uses [18,21,24–27], for the fabrication of 3D nanostructured materials with well-defined

physico-chemical features [28–35] and for the development of original cage-based materials with different porosity and host–guest chemistry [36–39].

The *Periodic Table of Metallasilsesquioxanes* already covers an abundant amount of metal elements included in the M-POSS structures, ranging from alkali and alkaline-earth metals [1,40–46] to metalloid ones [2,47–54], from transition and post-transition metals [21,23,43,50,55–59] to lanthanides [36,43,60–70] and actinides [41,43]. Transition metals, such as  $\text{Ti}^{4+}$ ,  $\text{Cr}^{3+}$ ,  $\text{Mn}^{2+}$ ,  $\text{Fe}^{3+}$ ,  $\text{Ni}^{2+}$ ,  $\text{Cu}^{2+}$  and  $\text{Pt}^{2+/4+}$ , have been investigated for their catalytic behavior, which shows high activity and selectivity in different reactions [71–73]. M-POSS combined with  $\text{Co}^{2+}$ ,  $\text{Ni}^{2+}$ ,  $\text{Cu}^{2+}$  and  $\text{Fe}^{3+/2+}$  have been studied for their unique paramagnetic properties, which are exploitable for the generation of spin-glass and single-molecule magnet systems [74–79].

In the last years, lanthanide-containing POSS (Ln-POSS) attracted growing attention from the scientific community for their potential uses in many fields, although the number of studies on this topic is still relatively small. Encapsulation of lanthanide ions within the cage of POSS [80] can circumvent their innate low thermal stability and mechanical resistance, leading to more stable lanthanide-doped silica-based systems. From an optical point of view, it is widely known that lanthanides exhibit sharp absorption bands with unique well-defined optical emissions in the NIR-UV-Vis range, long-lived excited state lifetimes and remarkable photostability [81,82]. Furthermore, lanthanide ions, such as  $\text{Gd}^{3+}$ ,  $\text{Dy}^{3+}$  and  $\text{Ho}^{3+}$ , possess specific chemical properties in terms of high effective magnetic moment and variable electronic relaxation times, which make them suitable for bioimaging [83–86] and electronic applications [87–92].

Ln-POSS are commonly prepared by reaction of the TriSilanol POSS with lanthanides salts. However, this procedure is designed to prepare M-POSS containing in the structure a single type of lanthanide ion. In this respect, samples with different chemical structures, from mononuclear cubic-like systems [39,43,63,65,67,69] to sandwich-type cages are developed [93–96]. On the contrary, the idea to include in the same inorganic cage two different metal ions with intrinsic properties is more promising but still rarely studied in the literature. Very recently, Professor J. Larionova and co-workers described a first example of bifunctional tetranuclear  $\text{Tb}^{3+}$ - $\text{Eu}^{3+}$  silsesquioxanes with a prism-like structure and good magnetic and luminescent properties [97,98]. This solid was prepared through a multi-step reaction procedure, starting with the lanthanides and silicon precursors. An analogous bifunctional structure containing both  $\text{Dy}^{3+}$  and  $\text{Y}^{3+}$  ions was also proposed by the same authors as potential single-molecule magnet system [99].

As an alternative to the compounds reported above, in this study, we propose a novel example of bifunctional double-decker POSS (DDSQ) that contains two different lanthanide centres ( $\text{Tb}^{3+}$  and  $\text{Eu}^{3+}$ ) in the same inorganic framework (TbEu-PhPOSS). The solid was prepared through a simple single-step reaction, starting with the TetraSilanolPhenyl POSS (PhPOSS) and the terbium and europium acetate precursors. This partially condensed POSS [100–105] possesses a pre-formed cubic cage with four diametrically opposite silanol groups (Figure S1) that are able to coordinate the two different lanthanide ions simultaneously. An analogous solid bearing in the structure  $\text{Tb}^{3+}$  ions was also prepared (Tb-PhPOSS). Finally, the chemical composition and the optical properties of the two samples were investigated.

## 2. Materials and Methods

### 2.1. Materials

#### 2.1.1. Synthesis of Tb-PhPOSS (1)

The Tb-PhPOSS sample was prepared by a corner-capping reaction of the partially condensed TetraSilanolPhenyl POSS (Figure S1) [100] with anhydrous terbium acetate, using a molar ratio of 2:1.

In detail, anhydrous terbium acetate ( $\text{Tb}(\text{CH}_3\text{COO})_3$ ; 78.5(5) mg, 0.234 mmol; Sigma-Aldrich, Burlington, MA, USA) was added with vigorous stirring to a solution of TetraSilanolPhenyl POSS (Ph-POSS; 500 mg, 0.467 mmol; Hybrid Plastics, Hattiesburg, MS, USA)

in 90 mL of anhydrous tetrahydrofuran (THF;  $\geq 99\%$ , Sigma-Aldrich, Burlington, MA, USA) in the presence of 272  $\mu\text{L}$  of triethylamine (TEA; 4.17 mmol;  $\geq 99\%$ , Sigma-Aldrich, Burlington, MA, USA). The reaction was carefully purged with nitrogen for 10 min. After the addition of the reactants, the temperature was fixed to 50  $^{\circ}\text{C}$ , and the mixture was stirred for 24 h. Then, the solvent was removed. The powder was washed with THF and ultrapure water to remove unreacted compounds and by-products, thus obtaining the Tb-PhPOSS (1) sample.

### 2.1.2. Synthesis of TbEu-PhPOSS (2)

The TbEu-PhPOSS sample was prepared following the same synthetic protocol described before for sample (1) with a relative molar ratio of the reactants of 2:0.5:0.5 (POSS:Tb<sup>3+</sup>:Eu<sup>3+</sup>).

In detail, a solid mixture of anhydrous terbium acetate (Tb(CH<sub>3</sub>COO)<sub>3</sub>; 39.32 mg, 0.117 mmol; Sigma-Aldrich, Burlington, MA, USA) and europium acetate (Eu(CH<sub>3</sub>COO)<sub>3</sub>; 38.50 mg, 0.117 mmol; Sigma-Aldrich, Burlington, MA, USA) was added to 90 mL of anhydrous tetrahydrofuran (THF;  $\geq 99\%$ , Sigma-Aldrich, Burlington, MA, USA), containing TetraSilanolPhenyl POSS (Ph-POSS; 500 mg, 0.467 mmol; Hybrid Plastics, Hattiesburg, MS, USA) and 272  $\mu\text{L}$  of triethylamine (TEA; 4.17 mmol;  $\geq 99\%$ , Sigma-Aldrich, Burlington, MA, USA). The reaction was carefully purged with nitrogen for 10 min. The temperature was fixed to 50  $^{\circ}\text{C}$ , and the mixture was stirred for 24 h. Then, the solvent was evaporated, and the final solid, hereafter named TbEu-PhPOSS (2), was washed with THF and water.

## 2.2. Analytical Methods

Elemental analyses were carried out on a Thermo Fisher Scientific X5 Series Inductively Coupled Plasma Mass Spectrometer (ICP-MS; Waltham, MA, USA). Before the analyses, the compounds were carefully mineralized by treating them with a mixture of nitric acid (5 mL) and hydrofluoric acid (5 mL) at 100  $^{\circ}\text{C}$  for 8 h.

CHN elemental analyses were accomplished with an EA3000 CHN Elemental Analyzer (EuroVector, Milano, Italy). Acetanilide, which was purchased by EuroVector (Milano, Italy), was used as the calibration standard (C% = 71.089, H% = 6.711, N% = 10.363).

Fourier-transform infrared spectroscopy (FT-IR) measurements were performed on a Bruker Equinox 55 Spectrometer operating in the 4000–400  $\text{cm}^{-1}$  range with a resolution of 4  $\text{cm}^{-1}$ . IR spectra of the solids mixed with potassium bromide (KBr) pellets were measured in absorbance mode at room temperature. The absorbance values are reported in absolute unit [a.u.].

X-ray powder diffractograms (XRPD) were collected on unoriented ground powders on a Bruker D8 Advance Powder Diffractometer, equipped with a Linxeye XE-T detector. The X-ray tube of the instrument operates with a Cu-K $_{\alpha 1}$  monochromatic radiation ( $\lambda = 1.54062 \text{ \AA}$ ), with the current intensity and operative electric potential difference set to 40 mA and 40 kV, respectively, and with variable primary divergent slits and primary and secondary Soller slits of 2.5 $^{\circ}$ . The X-ray profiles were recorded at room temperature in the 5–70 $^{\circ}$   $2\theta$  range with a coupled- $2\theta$ - $\theta$  method, fast and continuous scan mode, time per step/rate of 0.05 $^{\circ}$ /min, increment/step size of 0.02 $^{\circ}$  and with automatic air scatter and slits.

Photoluminescence (PL) spectra (excitation and emission) of the compounds at solid-state were recorded on a Horiba Jobin-Yvon Model IBH FL-322 Fluorolog 3 Spectrometer, equipped with a 450 W Xenon arc lamp, double grating excitation and emission monochromators (2.1  $\text{nm}\cdot\text{mm}^{-1}$  dispersion; 1200 grooves per mm) and a Hamamatsu Model R928 photomultiplier tube. Time-resolved measurements were carried out, instead, by using the time-correlated single-photon counting (TCSPC) option. A 370 nm SpectraLED laser was employed to excite the samples at solid-state and in H<sub>2</sub>O and D<sub>2</sub>O. The signal was collected using an IBH DataStation Hub photon counting module, while data analysis was accomplished with the commercial DAS6 software (HORIBA Jobin Yvon IBH Ltd., Glasgow, UK).

### 3. Results and Discussion

The two luminescent POSS, incorporating Tb<sup>3+</sup> and a combination of Tb<sup>3+</sup> and Eu<sup>3+</sup> ions, were prepared by a one-step corner-capping reaction between the PhPOSS and the lanthanide precursors. The reaction was performed under simple conditions, in anhydrous solvent THF, in the presence of a small amount of TEA at 50 °C for 24 h. During the reaction, the four reactive Si-OH groups of PhPOSS reacted with lanthanide ions' reactants.

The Tb<sup>3+</sup> and Eu<sup>3+</sup> contents in both samples were determined by an inductively coupled plasma mass spectrometry (ICP-MS), while the amount of carbon was quantified by a CHN analysis (Table 1). The amount of Tb<sup>3+</sup> ions was found to be 0.63 mmol/g and 0.26 mmol/g for Tb-PhPOSS and TbEu-PhPOSS, respectively, while the Eu<sup>3+</sup> loading was equal to 0.30 mmol/g in the bimetallic POSS. The carbon content was equivalent to 42.24 mmol/g and 41.30 mmol/g for Tb-PhPOSS and TbEu-PhPOSS, respectively, in agreement with the chemical composition of the reactant PhPOSS. By combining the data obtained from the ICP and CHN analyses, it was possible to extrapolate the number of lanthanide ions per POSS cage. In detail, for Tb-PhPOSS, we calculated a molar ratio between the number of cages and the Tb<sup>3+</sup> ion of 1.4. This could suggest that Tb-PhPOSS is composed by a polycondensed structure in which each Tb<sup>3+</sup> is shared by two coordinated POSS cages (Figure 1). A similar result was obtained for TbEu-PhPOSS, considering for the quantification the total amount of the two lanthanide ions embedded in the structure (Figure 1).

Additional structural information on the metal-containing POSS samples was obtained by infrared spectroscopy. IR spectra of the samples, recorded in the 4000–400 cm<sup>-1</sup> range, are reported in Figure 2. The vibrational profiles of Tb-PhPOSS and TbEu-PhPOSS are compared with the spectrum of PhPOSS sample.

**Table 1.** Amount of Tb<sup>3+</sup>, Eu<sup>3+</sup> and C elements (in mmol/g) in Tb-PhPOSS and TbEu-PhPOSS.

Sample	Tb <sup>3+</sup> Content [mmol/g]	Eu <sup>3+</sup> Content [mmol/g]	C Content [mmol/g]
Tb-PhPOSS	0.63	-	42.24
TbEu-PhPOSS	0.26	0.30	41.30

The IR spectrum of PhPOSS (Figure 2, a) shows the typical signals of phenyl groups at 3100–3000 cm<sup>-1</sup> (stretching of C-H groups) and at 1595, 1490 and 1430 cm<sup>-1</sup>, assigned to the stretching modes of C=C [100,106]. The main absorption of the POSS cage is detectable at 1100 cm<sup>-1</sup>, and it is ascribed to the asymmetric stretching of the siloxane (Si-O-Si) groups of the inorganic framework [100,106,107]. Finally, the absorptions at 3250 and 895 cm<sup>-1</sup> are characteristics of the stretching modes of OH and Si-OH functionalities, which are typical of partially condensed POSS molecules [100,106,107].

After reaction with the Tb<sup>3+</sup> precursor (Figure 2, b) or the mixture of terbium and europium salts (Figure 2, c), the IR spectra of both solids show a complete erosion of the bands located at 3250 and 895 cm<sup>-1</sup>, as a consequence of the condensation of Si-OH groups with the lanthanide ions. The bands of phenyl groups are still visible, proving that the organic groups attached to the POSS cage are preserved during the corner-capping reaction. Finally, it is worth noting that the band at 1100 cm<sup>-1</sup> appears more defined and narrower with respect to the POSS reactant. This is undoubtedly indicative of an orderly and regular organization of the Si-O-Si network, promoted by the presence of the lanthanide ions during the condensation reaction. This comment is qualitatively supported by the X-ray powder diffraction (XRPD) data shown in Figure 3.

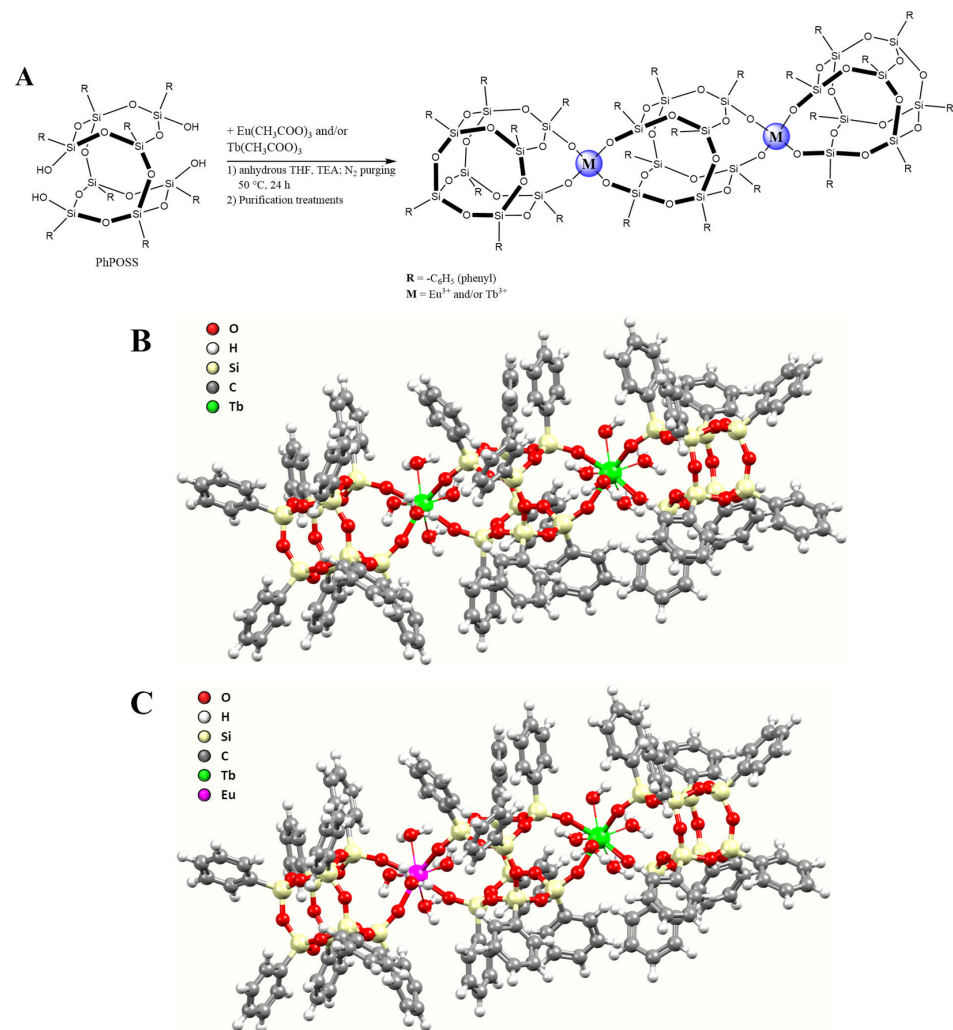


**Figure 1.** (A) Synthesis of metal-containing PhPOSS. Schematic view of a possible structure of Tb-PhPOSS (B) and TbEu-PhPOSS (C).

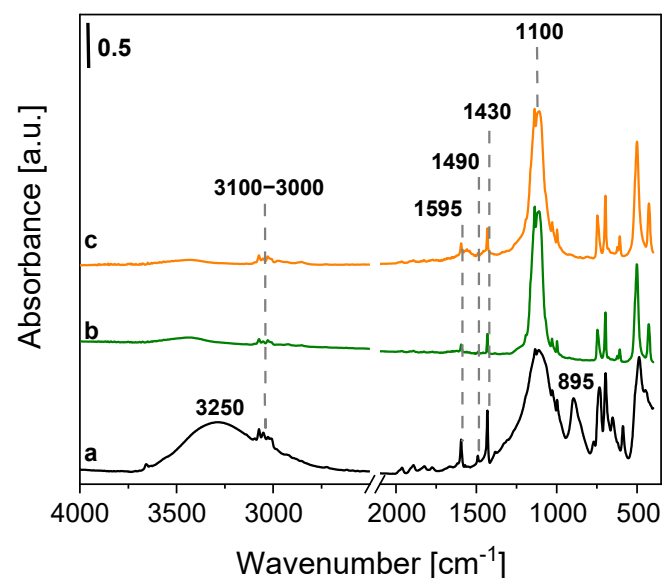


**Figure 2.** FT-IR spectra of PhPOSS (a), Tb-PhPOSS (b) and TbEu-PhPOSS (c), collected in KBr matrix (10 wt%).

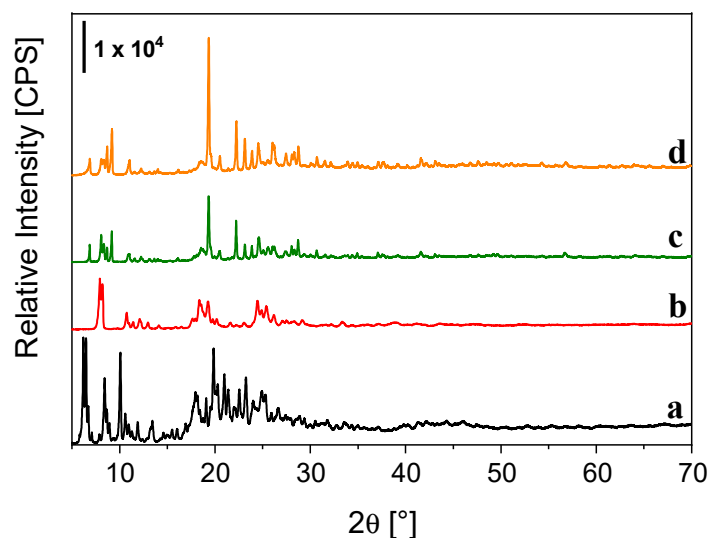


**Figure 3.** X-ray powder diffraction profiles of PhPOSS (a), the commercial condensed OctaPhenyl POSS (b), Tb-PhPOSS (c) and TbEu-PhPOSS (d). The diffractograms were collected in the 5–70°  $2\theta$  range.

The diffractogram of the PhPOSS is composed by well-resolved peaks in the 5–70°  $2\theta$  range, as is typically observed for crystalline POSS (Figure 3, a). After the corner-capping reaction, the X-ray profiles of Tb-PhPOSS and TbEu-PhPOSS show new well-defined peaks, and both profiles differ from that of PhPOSS and the analogous completely condensed OctaPhenyl POSS (Figure 3, b and Figure S2). The coordination of  $Tb^{3+}$  and  $Eu^{3+}$  ions promoted a different ordered structural arrangement of the POSS molecules with respect to the PhPOSS (Figure 3, c and d). Furthermore, the two diffraction patterns are comparable to each other, thus testifying that both Tb-PhPOSS and TbEu-PhPOSS have a similar crystallographic arrangement. More structural information can be obtained by single crystal X-ray diffraction, but, unfortunately, we did not obtain suitable crystals for the analysis. Furthermore, NMR analysis is difficult to apply to samples containing “shift agents”.

The photophysical properties of the luminescent Tb-PhPOSS and TbEu-PhPOSS products were carefully investigated by photoluminescence (PL) spectroscopy. The excitation spectra at solid-state of Tb-PhPOSS (Figure S3) and TbEu-PhPOSS (Figure 4A), measured at the most intense emission line of terbium at 545 nm, are essentially composed by the characteristic peaks of the intra- $4f^8$  electronic transitions of  $Tb^{3+}$ , assigned to:  ${}^7F_6-{}^5D_J$  ( $J = 1-4$ ),  ${}^7F_6-{}^5I_8$ ,  ${}^7F_6-{}^5F_{4-5}$ ,  ${}^7F_6-{}^5H_J$  ( $J = 4, 7$ ),  ${}^7F_6-{}^5L_J$  ( $J = 7-10$ ) and  ${}^7F_6-{}^5G_J$  ( $J = 3, 5, 6$ ) [108–110]. The maximum absorption band of  $Tb^{3+}$  displayed in both samples is located between ca. 280–290 nm, and it was ascribed to a combination of  ${}^7F_6-5d$  and  ${}^7F_6-{}^5I_8/{}^5F_{4-5}/{}^5H_4$  electronic transitions. The solid-state excitation spectrum of TbEu-PhPOSS, monitored at the most intense emission line of  $Eu^{3+}$  at 615 nm (Figure 4B), instead, showed (i) the presence of the same  $Tb^{3+}$  signals before indicated, and (ii) additional peaks ascribed to the intra- $4f^6$  electronic transitions of  $Eu^{3+}$  ( ${}^7F_0-{}^5H_J$ ,  ${}^7F_{0,1}-{}^5D_J$ ,  ${}^7F_0-{}^5G_J$  and  ${}^7F_0-{}^5L_J$ ), with a  $\lambda_{max}$  at 395 nm ( ${}^7F_0-{}^5L_6$ ) [108–111]. The presence of the  $Tb^{3+}$  transitions in Figure 4B represent a clear indication of the presence of a metal-to-metal energy transfer from  $Tb^{3+} \rightarrow Eu^{3+}$  ions [110,112–114].



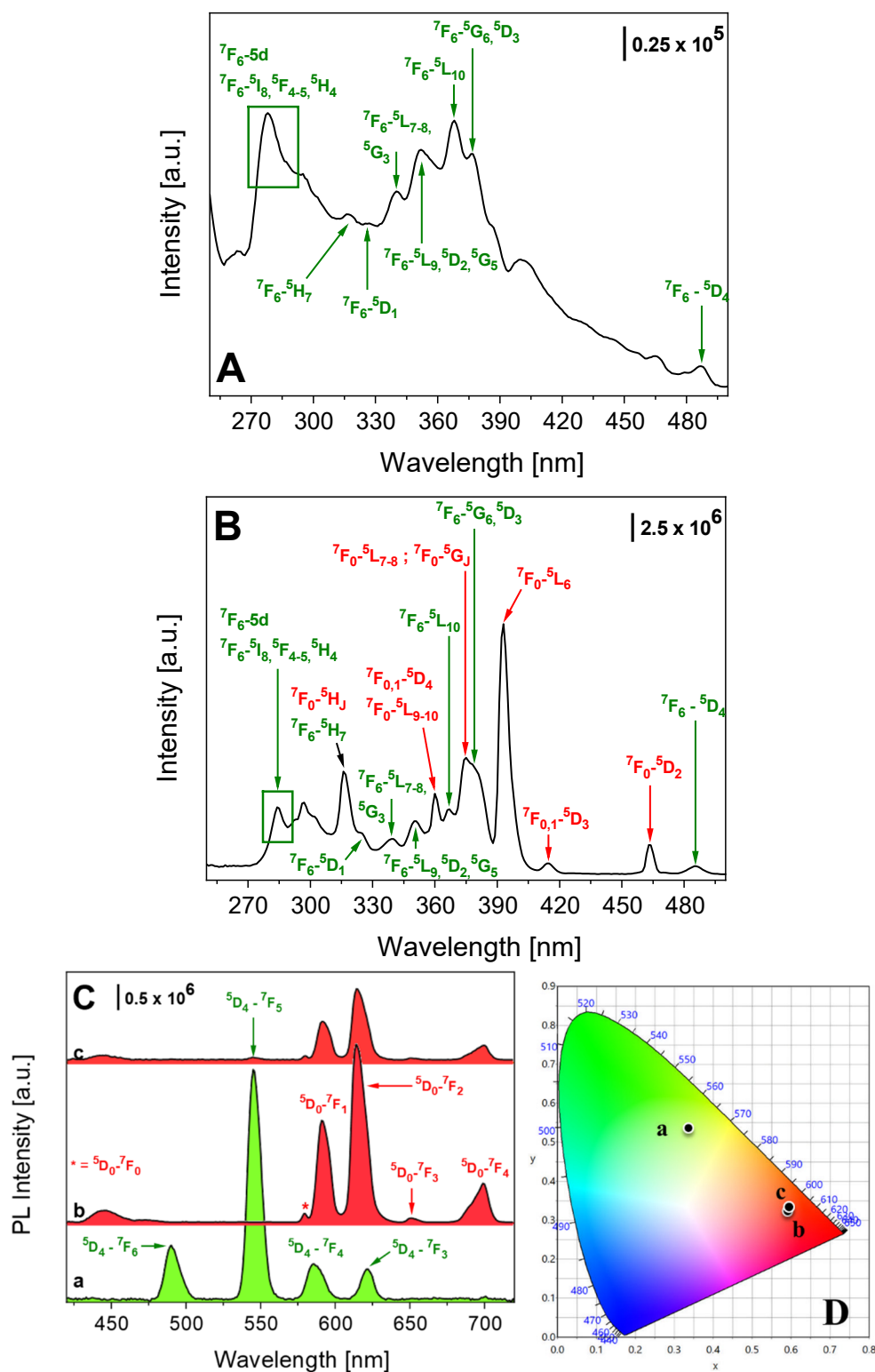


**Figure 4.** Excitation spectra at solid-state of TbEu-PhPOSS monitored at  $\lambda_{em} = 545$  nm (A) and  $\lambda_{em} = 615$  nm (B). (C) Emission spectra at solid-state of Tb-PhPOSS (a,  $\lambda_{exc} = 285$  nm) and TbEu-PhPOSS (b,  $\lambda_{exc} = 395$  nm, c,  $\lambda_{exc} = 285$  nm). The electronic transitions of terbium are marked in green colour, while those assigned to europium are in red, for more clarity. (D) CIE 1931 xy chromaticity diagrams derived from emission spectra in frame (C). The colour of each emission spectrum in frame (C) is associated with its corresponding xy coordinates (frame (D) and Table S2).

Further confirmation of the energy transfer process was obtained by collecting the solid-state emission spectra of TbEu-PhPOSS under irradiation at the  $\lambda_{\max}$  of  $\text{Eu}^{3+}$  at 395 nm (Figure 4C, b) and of  $\text{Tb}^{3+}$  at 285 nm (Figure 4C, c). The comparison with the photoluminescence spectrum of Tb-PhPOSS collected under excitation at 285 nm is reported in Figure 4C. The emission spectrum measured under excitation at 285 nm (Figure 4C, c) showed a very weak and broad emission peak at 545 nm, typical of  $\text{Tb}^{3+}$  ( $^5\text{D}_4 \rightarrow ^7\text{F}_5$ ) [108–110], together with the intense and characteristic emission bands of  $\text{Eu}^{3+}$  ( $^5\text{D}_0 \rightarrow ^7\text{F}_J$ ,  $J = 0-4$ ), with the most intense line centred at 615 nm ( $^5\text{D}_0 \rightarrow ^7\text{F}_2$ ) [108–111]. The photoluminescence of  $\text{Eu}^{3+}$  under excitation of  $\text{Tb}^{3+}$ , coupled with a marked decrease in the intensity of the main emission band of  $\text{Tb}^{3+}$  at 545 nm, testifies to the occurrence of the  $\text{Tb}^{3+} \rightarrow \text{Eu}^{3+}$  energy transfer process because the two metals are in close proximity [110,112–114].

The nature of the local chemical environment around the lanthanide centres was extrapolated from the emission spectra shown in Figure 4C. First, the  $\text{Eu}^{3+}$  sites appear to be heterogeneously distributed in the TbEu-PhPOSS sample, due to the presence of two weak peaks assigned to the  $^5\text{D}_0 \rightarrow ^7\text{F}_0$  electronic transition at 579 and 580 nm (Figure S4). This assumption is based on the fact that the number of distinct chemical domains around  $\text{Eu}^{3+}$  can be correlated to the multiplicity of the  $^5\text{D}_0 \rightarrow ^7\text{F}_0$  band, since its initial and final energy states are both non-degenerated [115]. In addition, the  $\text{Eu}^{3+}$  and  $\text{Tb}^{3+}$  ions in both solids are placed in a low symmetry environment with no inversion centre, as extrapolated by the high asymmetry factor ( $R$ ) values between  $1.4 \div 1.8$  for europium and  $1.0 \div 4.3$  for terbium (Table S1). The decrease in the  $R$  parameter from ca. 4.3 for Tb-PhPOSS (Figure 4C, a) to ca. 1.1 of TbEu-PhPOSS (Figure 4C, c), both under excitation at 285 nm, represents other evidence of the energy transfer process. The  $R$  factor was calculated from the intensity ratio of the electric-dipole  $^5\text{D}_0 \rightarrow ^7\text{F}_2$  on the magnetic-dipole  $^5\text{D}_0 \rightarrow ^7\text{F}_1$  for europium [116,117], while for terbium the ratio is  $^5\text{D}_4 \rightarrow ^7\text{F}_5 / ^5\text{D}_4 \rightarrow ^7\text{F}_6$  [118].

The photometric features of the Tb-PhPOSS and TbEu-POSS solids were obtained from their respective emission spectra, calculating the  $xy$  chromaticity coordinates and related Hex and RGB parameters according to CIE 1931 colour spaces (Figure 4D and Table S2) [119]. The direct excitation of  $\text{Eu}^{3+}$  sites at 395 nm in TbEu-PhPOSS led to a red emission colour (point b in Figure 4D), and, after excitation at 285 nm ( $\lambda_{\max}$  of  $\text{Tb}^{3+}$ ), the bimetallic sample showed a very small blue-shift of its emission towards a slightly more orange-red colour (point c in Figure 4D). For reference, the colour associated with the emission of Tb-PhPOSS is light green (point a in Figure 4D).

The average hydration state of  $\text{Tb}^{3+}$  ions ( $q^{\text{Tb}}$ ) in the Tb-PhPOSS and of  $\text{Eu}^{3+}$  ions ( $q^{\text{Eu}}$ ) in the TbEu-PhPOSS were estimated by measuring, via time-resolved fluorescence spectroscopy, the experimental lifetimes ( $\tau$ ) associated with the transitions at 545 and 615 nm, respectively, in  $\text{H}_2\text{O}$  and  $\text{D}_2\text{O}$  under excitation at 370 nm. The  $q^{Ln}$  values for  $\text{Tb}^{3+}$  and  $\text{Eu}^{3+}$  were calculated by applying the following Equations (1) and (2) [120–123].

$$q^{\text{Eu}} = 1.20 \cdot (1/\tau_{\text{H}_2\text{O}} - 1/\tau_{\text{D}_2\text{O}} - 0.25) \quad (1)$$

$$q^{\text{Tb}} = 4.26 \cdot (1/\tau_{\text{H}_2\text{O}} - 1/\tau_{\text{D}_2\text{O}} - 0.06) \quad (2)$$

The photoluminescence decay curves of the  $^5\text{D}_4$  excited state of  $\text{Tb}^{3+}$  (Figure S5A,B) and  $^5\text{D}_0$  excited state of  $\text{Eu}^{3+}$  (Figure S5C,D), fitted with a bi-exponential function, suggest the presence of ca. five water molecules in the first coordination sphere of both lanthanide ions (Table S3). The results are consistent with the hypothetical structure of the samples described before, considering that the two lanthanide ions can easily expand their coordination sphere up to coordination number values of 8–9 [108,124].

The  $\text{Tb}^{3+}$ - $\text{Eu}^{3+}$  energy transfer mechanism was analysed in more detail by collecting the lifetime values ( $\tau$ ) at solid-state of Tb-PhPOSS (donor system, D) and TbEu-PhPOSS (donor-acceptor system, DA). The intensity decay curves of  $^5\text{D}_4$  excited state of  $\text{Tb}^{3+}$  were measured for both samples at  $\lambda_{\text{em}}$  of 545 nm, under excitation at 370 nm (Figure S6). The curves were well fitted with a bi-exponential function, and, from these, the average  $\tau$  values were derived. The energy transfer efficiency ( $E_{\text{EnT}}$ ) and rate ( $k_{\text{EnT}}$ ) parameters were then



calculated by using the average lifetimes measured at 545 nm of the donor ion ( $\text{Tb}^{3+}$ ) in the presence ( $\tau_{DA}$ , Figure S6B) or absence ( $\tau_D$ , Figure S6A) of the acceptor one ( $\text{Eu}^{3+}$ ), by using Equations (3) and (4) [112,113,125,126].

$$k_{EnT} [s^{-1}] = \left( \frac{1}{\tau_{DA}} - \frac{1}{\tau_D} \right) \quad (3)$$

$$E_{EnT} (o \eta_{sens}) [\%] = \left( 1 - \frac{\tau_{DA}}{\tau_D} \right) \cdot 100 \quad (4)$$

The results, reported in Table 2, showed a  $\text{Tb}^{3+} \rightarrow \text{Eu}^{3+}$  energy transfer efficiency value of ca. 62%, with a rate constant of the process equal to  $4.09 \times 10^3 \text{ s}^{-1}$ , comparable to those observed for other inorganic materials functionalized with both  $\text{Tb}^{3+}$  and  $\text{Eu}^{3+}$  ions [110,112,114,127].

**Table 2.** Experimental lifetimes ( $\tau$ ) of Tb-PhPOSS (D) and TbEu-PhPOSS (DA), collected by monitoring the main emission of  $\text{Tb}^{3+}$  at 545 nm ( $^5\text{D}_4\text{-}^7\text{F}_5$  electronic transition) under irradiation at 370 nm. The  $\text{Tb}^{3+} \rightarrow \text{Eu}^{3+}$  energy transfer rate ( $k_{EnT}$ ) and efficiency ( $E_{EnT}$ ) parameters are also reported.

$\tau_D$ [s]	$\tau_{DA}$ [s]	$k_{EnT}$ [ $\text{s}^{-1}$ ]	$E_{EnT}$ [%]
$3.88 \times 10^{-4}$	$1.50 \times 10^{-4}$	$4.09 \times 10^3$	61.34

#### 4. Conclusions

In this study, novel completely condensed luminescent double-decker POSS solids functionalized with  $\text{Tb}^{3+}$  and a combination of  $\text{Tb}^{3+}$  and  $\text{Eu}^{3+}$  ions were prepared by a simple one-pot corner-capping reaction under mild conditions. The synthetic protocol adopted in this work allows for obtainment of a polycondensed POSS with the following properties: (i) ordered architecture of the POSS structure; (ii) a well-defined molar ratio of cage units and the lanthanide ions in both samples; (iii) each lanthanide ion is connected to different POSS cages with an expansion of the coordination state with five inner sphere water molecules; (iv) tunable emission properties for the bimetallic POSS and (v) remarkable energy transfer from the  $\text{Tb}^{3+}$  to  $\text{Eu}^{3+}$  centers in terms of efficiency and the process rate. The optical properties of both Tb-PhPOSS and TbEu-PhPOSS solids make them ideal candidates for the fabrication of novel optical thermometers and sensor devices. Further studies are currently underway to evaluate the effect of the reaction's stoichiometry on the structure and chemical composition of the final samples.

**Supplementary Materials:** The following supporting information can be downloaded at <https://www.mdpi.com/article/10.3390/pr10040758/s1>. Figure S1: Schematic view of the structure of the partially condensed PhPOSS.; Figure S2: Schematic view of the structure of the completely condensed OctaPhenyl POSS.; Figure S3: Excitation spectrum at solid-state of Tb-PhPOSS monitored at 545 nm.; Figure S4: Magnification of the region associated with the  $^5\text{D}_0\text{-}^7\text{F}_0$  electronic transition of  $\text{Eu}^{3+}$  in the solid-state emission spectra of TbEu-PhPOSS reported in Figure 4C, measured under excitation at 395 nm (a) and 285 nm (b).; Figure S5: Normalized PL  $\text{Tb}^{3+} ^5\text{D}_4\text{-}^7\text{F}_5$  (545 nm) intensity decay over time of Tb-PhPOSS in  $\text{H}_2\text{O}$  (A) and  $\text{D}_2\text{O}$  (B) under irradiation at 370 nm. Normalized PL  $\text{Eu}^{3+} ^5\text{D}_0\text{-}^7\text{F}_2$  (615 nm) intensity decay over time of TbEu-PhPOSS in  $\text{H}_2\text{O}$  (C) and  $\text{D}_2\text{O}$  (D), under irradiation at 370 nm. The curve's fitting was performed with a bi-exponential function (black lines). The  $\chi^2$  and RSS (residual sum of squares) values are reported in the table below.; Figure S6: Normalized PL  $\text{Tb}^{3+} ^5\text{D}_4\text{-}^7\text{F}_5$  (545 nm) intensity decay over time of Tb-PhPOSS (A) and TbEu-PhPOSS (B), collected at the solid-state under irradiation at 370 nm. The curve's fitting was performed with a bi-exponential function (black lines). The  $\chi^2$  and RSS (residual sum of squares) values are reported in the table below.; Table S1: Asymmetry factors ( $R$ ) of  $\text{Tb}^{3+}$  and  $\text{Eu}^{3+}$  for Tb-PhPOSS and TbEu-PhPOSS, under irradiation at 285 nm ( $\text{Tb}^{3+}$ ) and 395 nm ( $\text{Eu}^{3+}$ ), calculated from the solid-state emission spectra reported in Figure 4C.; Table S2: Photometric data, in accordance with CIE 1931 colour spaces, for Tb-PhPOSS and TbEu-PhPOSS, extrapolated from the solid-state emission spectra shown in Figure 4C.; Table S3: Hydration state of  $\text{Tb}^{3+}$  ( $q^{\text{Tb}}$ ) and  $\text{Eu}^{3+}$  ( $q^{\text{Eu}}$ ) in Tb-PhPOSS and TbEu-PhPOSS, respectively,

obtained from the experimental lifetimes ( $t$ ) measured in H<sub>2</sub>O and D<sub>2</sub>O. The lifetimes were collected at 545 nm for terbium and 615 nm for europium, under excitation at 370 nm with a SpectraLED source.

**Author Contributions:** Conceptualization, S.M., C.B. and F.C.; methodology, S.M., C.B. and F.C.; formal analysis, S.M.; investigation, S.M.; data curation, S.M. and F.C.; writing—original draft preparation, S.M.; writing—review and editing, C.B. and F.C. All authors have read and agreed to the published version of the manuscript.

**Funding:** Financial support from Università del Piemonte Orientale (FAR-2019) is acknowledged.

**Institutional Review Board Statement:** Not applicable.

**Informed Consent Statement:** Not applicable.

**Data Availability Statement:** Not applicable.

**Acknowledgments:** The authors are fully grateful to Elena Perin (DiSIT, Università del Piemonte Orientale, Alessandria, Italy) for the ICP-MS analyses and to Gualtiero Borzoni for his help in the experimental analyses.

**Conflicts of Interest:** The authors declare no conflict of interest.

## References

1. Lorenz, V.; Gießmann, S.; Gun'Ko, Y.K.; Fischer, A.K.; Gilje, J.W.; Edelmann, F.T. Fully Metalated Silsesquioxanes: Building Blocks for the Construction of Catalyst Models. *Angew. Chem. Int. Ed.* **2004**, *43*, 4603–4606. [[CrossRef](#)] [[PubMed](#)]
2. Feher, F.J.; Budzichowski, T.A.; Rahimian, K.; Ziller, J.W. Reactions of incompletely-condensed silsesquioxanes with pentamethylantimony: A new synthesis of metallasilsesquioxanes with important implications for the chemistry of silica surfaces. *J. Am. Chem. Soc.* **1992**, *114*, 3859–3866. [[CrossRef](#)]
3. Crocker, M.; Herold, R.H.M.; Orpen, A.G.; Overgaag, M.T.A. Synthesis and characterisation of titanium silsesquioxane complexes: Soluble models for the active site in titanium silicate epoxidation catalysts. *J. Chem. Soc. Dalton Trans.* **1999**, 3791–3804. [[CrossRef](#)]
4. Wada, K.; Bundo, M.; Nakabayashi, D.; Itayama, N.; Kondo, T.; Mitsudo, T.-A. Synthesis of Novel Group 4 Metallocene-Containing Silsesquioxanes with a Vinyl Group. *Chem. Lett.* **2000**, *29*, 628–629. [[CrossRef](#)]
5. Abbenhuis, H.C.L. Advances in Homogeneous and Heterogeneous Catalysis with Metal-Containing Silsesquioxanes. *Chem. Eur. J.* **2000**, *6*, 25–32. [[CrossRef](#)]
6. Ward, A.J.; Masters, A.F.; Maschmeyer, T. Metallasilsesquioxanes: Molecular Analogues of Heterogeneous Catalysts. In *Applications of Polyhedral Oligomeric Silsesquioxanes*; Hartmann-Thompson, C., Ed.; Advances in Silicon Science; Springer: Dordrecht, The Netherlands, 2011; pp. 135–166. ISBN 978-90-481-3787-9.
7. Roesky, H.W.; Anantharaman, G.; Chandrasekhar, V.; Jancik, V.; Singh, S. Control of Molecular Topology and Metal Nuclearity in Multimetallic Assemblies: Designer Metallosiloxanes Derived from Silanetriols. *Chem. A Eur. J.* **2004**, *10*, 4106–4114. [[CrossRef](#)]
8. Levitsky, M.M.; Bilyachenko, A.N. Modern concepts and methods in the chemistry of polyhedral metallasiloxanes. *Coord. Chem. Rev.* **2016**, *306*, 235–269. [[CrossRef](#)]
9. Harrison, P.G. Silicate cages: Precursors to new materials. *J. Organomet. Chem.* **1997**, *542*, 141–183. [[CrossRef](#)]
10. Pescarmona, P.P.; Maschmeyer, T. Review: Oligomeric Silsesquioxanes: Synthesis, Characterization and Selected Applications. *Aust. J. Chem.* **2001**, *54*, 583–596. [[CrossRef](#)]
11. Baney, R.H.; Itoh, M.; Sakakibara, A.; Suzuki, T. Silsesquioxanes. *Chem. Rev.* **1995**, *95*, 1409–1430. [[CrossRef](#)]
12. Cordes, D.B.; Lickiss, P.D.; Rataboul, F. Recent Developments in the Chemistry of Cubic Polyhedral Oligosilsesquioxanes. *Chem. Rev.* **2010**, *110*, 2081–2173. [[CrossRef](#)]
13. Feher, F.J.; Newman, D.A.; Walzer, J.F. Silsesquioxanes as models for silica surfaces. *J. Am. Chem. Soc.* **1989**, *111*, 1741–1748. [[CrossRef](#)]
14. Ye, M.; Wu, Y.; Zhang, W.; Yang, R. Synthesis of incompletely caged silsesquioxane (T7-POSS) compounds via a versatile three-step approach. *Res. Chem. Intermed.* **2018**, *44*, 4277–4294. [[CrossRef](#)]
15. Fan, L.; Wang, X.; Wu, D. Polyhedral Oligomeric Silsesquioxanes (POSS)-Based Hybrid Materials: Molecular Design, Solution Self-Assembly and Biomedical Applications. *Chin. J. Chem.* **2021**, *39*, 757–774. [[CrossRef](#)]
16. Imoto, H.; Ueda, Y.; Sato, Y.; Nakamura, M.; Mitamura, K.; Watase, S.; Naka, K. Corner- and Side-Opened Cage Silsesquioxanes: Structural Effects on the Materials Properties. *Eur. J. Inorg. Chem.* **2020**, *2020*, 737–742. [[CrossRef](#)]
17. Pan, G. Polyhedral Oligomeric Silsesquioxane (POSS). In *Physical Properties of Polymers Handbook*; Mark, J.E., Ed.; Springer: New York, NY, USA, 2007; pp. 577–584. ISBN 978-0-387-69002-5.
18. Henig, J.; Tóth, É.; Engelmann, J.; Gottschalk, S.; Mayer, H.A. Macrocyclic Gd<sup>3+</sup> Chelates Attached to a Silsesquioxane Core as Potential Magnetic Resonance Imaging Contrast Agents: Synthesis, Physicochemical Characterization, and Stability Studies. *Inorg. Chem.* **2010**, *49*, 6124–6138. [[CrossRef](#)]
19. Köytepe, S.; Demirel, M.H.; Gültek, A.; Seçkin, T. Metallo-supramolecular materials based on terpyridine-functionalized polyhedral silsesquioxane. *Polym. Int.* **2014**, *63*, 778–787. [[CrossRef](#)]

20. Li, Y.; Dong, X.-H.; Zou, Y.; Wang, Z.; Yue, K.; Huang, M.; Liu, H.; Feng, X.; Lin, Z.; Zhang, W.; et al. Polyhedral oligomeric silsesquioxane meets “click” chemistry: Rational design and facile preparation of functional hybrid materials. *Polymer* **2017**, *125*, 303–329. [[CrossRef](#)]
21. Lorenz, V.; Fischer, A.; Gießmann, S.; Gilje, J.W.; Gun'Ko, Y.; Jacob, K.; Edelmann, F.T. Disiloxanediolates and polyhedral metallasilsesquioxanes of the early transition metals and f-elements. *Coord. Chem. Rev.* **2000**, *206–207*, 321–368. [[CrossRef](#)]
22. Du, Y.; Liu, H. Cage-like silsesquioxanes-based hybrid materials. *Dalton Trans.* **2020**, *49*, 5396–5405. [[CrossRef](#)]
23. Wada, K.; Mitsudo, T.-A. Preparation of Novel Materials for Catalysts Utilizing Metal-Containing Silsesquioxanes. *Catal. Surv. Asia* **2005**, *9*, 229–241. [[CrossRef](#)]
24. Lichtenhan, J.D. Polyhedral Oligomeric Silsesquioxanes: Building Blocks for Silsesquioxane-Based Polymers and Hybrid Materials. *Comments Inorg. Chem.* **1995**, *17*, 115–130. [[CrossRef](#)]
25. Olivero, F.; Renò, F.; Carniato, F.; Rizzi, M.; Cannas, M.; Marchese, L. A novel luminescent bifunctional POSS as a molecular platform for biomedical applications. *Dalton Trans.* **2012**, *41*, 7467–7473. [[CrossRef](#)]
26. Kaneshiro, T.L.; Jeong, E.-K.; Morrell, G.; Parker, D.L.; Lu, Z.-R. Synthesis and Evaluation of Globular Gd-DOTA-Monoamide Conjugates with Precisely Controlled Nanosizes for Magnetic Resonance Angiography. *Biomacromolecules* **2008**, *9*, 2742–2748. [[CrossRef](#)] [[PubMed](#)]
27. Ghanbari, H.; Cousins, B.G.; Seifalian, A. A Nanocage for Nanomedicine: Polyhedral Oligomeric Silsesquioxane (POSS). *Macromol. Rapid Commun.* **2011**, *32*, 1032–1046. [[CrossRef](#)] [[PubMed](#)]
28. Duchateau, R. Incompletely Condensed Silsesquioxanes: Versatile Tools in Developing Silica-Supported Olefin Polymerization Catalysts. *Chem. Rev.* **2002**, *102*, 3525–3542. [[CrossRef](#)] [[PubMed](#)]
29. Venegoni, I.; Carniato, F.; Olivero, F.; Bisio, C.; Pira, N.L.; Lambertini, V.G.; Marchese, L. A novel electroluminescent PPV copolymer and silsesquioxane nanocomposite film for the preparation of efficient PLED devices. *Nanotechnology* **2012**, *23*, 435702. [[CrossRef](#)] [[PubMed](#)]
30. Carniato, F.; Bisio, C.; Gatti, G.; Boccaleri, E.; Bertinetti, L.; Coluccia, S.; Monticelli, O.; Marchese, L. Titanosilsesquioxanes Embedded in Synthetic Clay as a Hybrid Material for Polymer Science. *Angew. Chem. Int. Ed.* **2009**, *48*, 6059–6061. [[CrossRef](#)]
31. Zhou, H.; Ye, Q.; Xu, J. Polyhedral oligomeric silsesquioxane-based hybrid materials and their applications. *Mater. Chem. Front.* **2017**, *1*, 212–230. [[CrossRef](#)]
32. Provatas, A.; Luft, M.; Mu, J.C.; White, A.H.; Matisons, J.G.; Skelton, B. Silsesquioxanes: Part I: A key intermediate in the building of molecular composite materials. *J. Organomet. Chem.* **1998**, *565*, 159–164. [[CrossRef](#)]
33. Wang, M.; Chi, H.; Joshy, K.S.; Wang, F. Progress in the Synthesis of Bifunctionalized Polyhedral Oligomeric Silsesquioxane. *Polymers* **2019**, *11*, 2098. [[CrossRef](#)] [[PubMed](#)]
34. DeArmitt, C. Polyhedral Oligomeric Silsesquioxanes in Plastics. In *Applications of Polyhedral Oligomeric Silsesquioxanes*; Hartmann-Thompson, C., Ed.; Advances in Silicon Science; Springer: Dordrecht, The Netherlands, 2011; pp. 209–228. ISBN 978-90-481-3787-9.
35. Brandhorst, H.W. Polyhedral Oligomeric Silsesquioxanes in Space Applications. In *Applications of Polyhedral Oligomeric Silsesquioxanes*; Hartmann-Thompson, C., Ed.; Advances in Silicon Science; Springer: Dordrecht, The Netherlands, 2011; pp. 327–361. ISBN 978-90-481-3787-9.
36. Marchesi, S.; Carniato, F.; Marchese, L.; Boccaleri, E. Luminescent Mesoporous Silica Built through Self-Assembly of Polyhedral Oligomeric Silsesquioxane and Europium(III) Ions. *ChemPlusChem* **2015**, *80*, 915–918. [[CrossRef](#)] [[PubMed](#)]
37. Lorenz, V.; Edelmann, F.T. Metallasilsesquioxanes. In *Advances in Organometallic Chemistry*; West, R., Hill, A.F., Stone, F.G.A., Eds.; Academic Press: Cambridge, MA, USA, 2005; Volume 53, pp. 101–153.
38. Murugavel, R.; Voigt, A.; Walawalkar, M.G.; Roesky, H.W. Hetero- and Metallasiloxanes Derived from Silanediols, Disilanol, Silanetriols, and Trisilanol. *Chem. Rev.* **1996**, *96*, 2205–2236. [[CrossRef](#)] [[PubMed](#)]
39. Hanssen, R.W.J.M.; van Santen, R.A.; Abbenhuis, H.C.L. The Dynamic Status Quo of Polyhedral Silsesquioxane Coordination Chemistry. *Eur. J. Inorg. Chem.* **2004**, *2004*, 675–683. [[CrossRef](#)]
40. Ye, X.; Li, J.; Zhang, W.; Yang, R.; Li, J. Fabrication of eco-friendly and multifunctional sodium-containing polyhedral oligomeric silsesquioxane and its flame retardancy on epoxy resin. *Compos. Part B Eng.* **2020**, *191*, 107961. [[CrossRef](#)]
41. Gießmann, S.; Lorenz, V.; Liebing, P.; Hilfert, L.; Fischer, A.; Edelmann, F.T. Synthesis and structural study of new metallasilsesquioxanes of potassium and uranium. *Dalton Trans.* **2017**, *46*, 2415–2419. [[CrossRef](#)]
42. Prigyai, N.; Chanmungkalakul, S.; Ervithayasuporn, V.; Yodsins, N.; Jungsuttiwong, S.; Takeda, N.; Unno, M.; Boonmak, J.; Kiatkamjornwong, S. Lithium-Templated Formation of Polyhedral Oligomeric Silsesquioxanes (POSS). *Inorg. Chem.* **2019**, *58*, 15110–15117. [[CrossRef](#)]
43. Lorenz, V.; Edelmann, F.T. Dimeric Silsesquioxanes and Metallasilsesquioxanes—En route to large, welldefined Si-O-assemblies. *Z. Anorg. Allg. Chem.* **2004**, *630*, 1147–1157. [[CrossRef](#)]
44. Lorenz, V.; Fischer, A.; Edelmann, F.T. Silsesquioxane chemistry, 6: The first beryllium silsesquioxane: Synthesis and structure of [Cy7Si7O12BeLi]2·2THF. *Inorg. Chem. Commun.* **2000**, *3*, 292–295. [[CrossRef](#)]
45. Maxim, N.; Magusin, P.; Kooyman, P.; van Wolput, J.H.; van Santen, A.R.A.; Abbenhuis, H.C.L. Microporous Mg–Si–O and Al–Si–O Materials Derived from Metal Silsesquioxanes. *Chem. Mater.* **2001**, *13*, 2958–2964. [[CrossRef](#)]
46. Hanssen, R.W.J.M.; Meetsma, A.; van Santen, R.A.; Abbenhuis, H.C.L. Synthesis, Structural Characterization, and Transmetalation Reactions of a Tetranuclear Magnesium Silsesquioxane Complex. *Inorg. Chem.* **2001**, *40*, 4049–4052. [[CrossRef](#)] [[PubMed](#)]

47. Astakhov, G.S.; Levitsky, M.M.; Zubavichus, Y.V.; Khrustalev, V.N.; Titov, A.A.; Dorovatovskii, P.V.; Smol'Yakov, A.F.; Shubina, E.S.; Kirillova, M.V.; Kirillov, A.M.; et al. Cu- $\zeta$ - and Cu- $\eta$ -Cage Sil- and Germanesquioxanes: Synthetic and Structural Features, Oxidative Rearrangements, and Catalytic Activity. *Inorg. Chem.* **2021**, *60*, 8062–8074. [[CrossRef](#)] [[PubMed](#)]
48. Zhai, B.; Zhu, S.; Tian, Q.; Li, N.; Yan, M.; Henderson, M.J. Aggregated germanium saponite: Removal and retention of polymeric thorium and uranium complexes. *Appl. Clay Sci.* **2021**, *216*, 106382. [[CrossRef](#)]
49. Grzelak, M.; Frackowiak, D.; Marciniak, B. Vinyl-Functionalized Silsesquioxanes and Germanesquioxanes. *Eur. J. Inorg. Chem.* **2017**, *2017*, 3337–3342. [[CrossRef](#)]
50. Gerritsen, G.; Duchateau, R.; van Santen, A.R.A.; Yap, G.P.A. Boron, Aluminum, and Gallium Silsesquioxane Compounds, Homogeneous Models for Group 13 Element-Containing Silicates and Zeolites. *Organometallics* **2003**, *22*, 100–110. [[CrossRef](#)]
51. Feher, F.J.; Budzichowski, T.A.; Ziller, J.W. Synthesis, reactivity, and dynamic behavior of a boron-containing silsesquioxane. *Inorg. Chem.* **1992**, *31*, 5100–5105. [[CrossRef](#)]
52. Feher, F.J.; Budzichowski, T.A. Heterosilsesquioxanes: Synthesis and characterization of Group 15 containing polyhedral oligosilsesquioxanes. *Organometallics* **1991**, *10*, 812–815. [[CrossRef](#)]
53. Zak, P.; Frackowiak, D.; Grzelak, M.; Bołt, M.; Kubicki, M.; Marciniak, B. Olefin Metathesis of Vinylgermanium Derivatives as Method for the Synthesis of Functionalized Cubic and Double-Decker Germanesquioxanes. *Adv. Synth. Catal.* **2016**, *358*, 3265–3276. [[CrossRef](#)]
54. Levitsky, M.M.; Zubavichus, Y.V.; Korlyukov, A.A.; Khrustalev, V.; Shubina, E.; Bilyachenko, A.N. Silicon and Germanium-Based Sesquioxanes as Versatile Building Blocks for Cage Metallacomplexes. A Review. *J. Clust. Sci.* **2019**, *30*, 1283–1316. [[CrossRef](#)]
55. Kaźmierczak, J.; Kuciński, K.; Stachowiak, H.; Hreczycho, G. Introduction of Boron Functionalities into Silsesquioxanes: Novel Independent Methodologies. *Chem. A Eur. J.* **2018**, *24*, 2509–2514. [[CrossRef](#)]
56. Besselink, R.; Venkatachalam, S.; Van Wüllen, L.; Elshof, J.E.T. Incorporation of niobium into bridged silsesquioxane based silica networks. *J. Sol Gel Sci. Technol.* **2014**, *70*, 473–481. [[CrossRef](#)]
57. García, C.; Gómez, M.; Gómez-Sal, P.; Hernández, J.M. Monocyclopentadienyl(niobium) Compounds with Imido and Silsesquioxane Ligands: Synthetic, Structural and Reactivity Studies. *Eur. J. Inorg. Chem.* **2009**, *2009*, 4401–4415. [[CrossRef](#)]
58. Feher, F.J.; Blanski, R.L. Olefin polymerization by vanadium-containing silsesquioxanes: Synthesis of a dialkyl-oxo-vanadium(V) complex that initiates ethylene polymerization. *J. Am. Chem. Soc.* **1992**, *114*, 5886–5887. [[CrossRef](#)]
59. Feher, F.J.; Walzer, J.F. Synthesis and characterization of vanadium-containing silsesquioxanes. *Inorg. Chem.* **1991**, *30*, 1689–1694. [[CrossRef](#)]
60. Annand, J.; Aspinall, H.C. Lanthanide silsesquioxanes: Monomeric and functionalised complexes. *J. Chem. Soc. Dalton Trans.* **2000**, 1867–1871. [[CrossRef](#)]
61. Annand, J.; Aspinall, H.C.; Steiner, A. Novel Heterometallic Lanthanide Silsesquioxane. *Inorg. Chem.* **1999**, *38*, 3941–3943. [[CrossRef](#)]
62. Wang, Y.; Lin, N. Highly transparent and luminescent lanthanide ion-containing bridged polysilsesquioxanes. *Photochem. Photobiol. Sci.* **2011**, *10*, 42–47. [[CrossRef](#)]
63. Marchesi, S.; Carniato, F.; Boccaleri, E. Synthesis and characterisation of a novel europium(iii)-containing heptaisobutyl-POSS. *New J. Chem.* **2014**, *38*, 2480–2485. [[CrossRef](#)]
64. Marchesi, S.; Bisio, C.; Boccaleri, E.; Carniato, F. A Luminescent Polysilsesquioxane Obtained by Self-Condensation of Anionic Polyhedral Oligomeric Silsesquioxanes (POSS) and Europium(III) Ions. *ChemPlusChem* **2020**, *85*, 176–182. [[CrossRef](#)]
65. Xu, Q.; Li, Z.; Chen, M.; Li, H. Synthesis and luminescence of octacarboxy cubic polyhedral oligosilsesquioxanes coordinated with terbium. *CrystEngComm* **2016**, *18*, 177–182. [[CrossRef](#)]
66. Kumar, B.P.; Kumar, A.P.; Bindu, P.H.; Mukherjee, K.; Patra, A.S. Red Light Emission of POSS Triol Chelated with Europium. *Asian J. Nanosci. Mater.* **2019**, *2*, 244–256.
67. Lorenz, V.; Edelmann, A.; Gießmann, S.; Hrib, C.G.; Blaurock, S.; Edelmann, F.T. Disiloxanediolates and Metallasilsesquioxanes of the Rare Earth Elements. *Z. Anorg. Allg. Chem.* **2010**, *636*, 2172–2191. [[CrossRef](#)]
68. Yi, S.S.; Jung, J.Y. Rare earth Doped organic–inorganic hybrid polyhedral oligomeric silsesquioxane phosphors applied for flexible sheet and anti-counterfeiting. *Mater. Express* **2021**, *11*, 1732–1738. [[CrossRef](#)]
69. Lorenz, V.; Blaurock, S.; Hrib, C.G.; Edelmann, F.T. Coupling of Silsesquioxane Cages in the Coordination Sphere of Erbium. *Eur. J. Inorg. Chem.* **2010**, *2010*, 2605–2608. [[CrossRef](#)]
70. Willauer, A.R.; Dabrowska, A.M.; Scopelliti, R.; Mazzanti, M. Structure and small molecule activation reactivity of a metallasilsesquioxane of divalent ytterbium. *Chem. Commun.* **2020**, *56*, 8936–8939. [[CrossRef](#)] [[PubMed](#)]
71. Levitsky, M.M.; Yalymov, A.I.; Kulakova, A.N.; Petrov, A.A.; Bilyachenko, N. Cage-like metallasilsesquioxanes in catalysis: A review. *J. Mol. Catal. A Chem.* **2017**, *426*, 297–304. [[CrossRef](#)]
72. Levitsky, M.M.; Bilyachenko, A.N.; Shul'Pin, G.B. Oxidation of C-H compounds with peroxides catalyzed by polynuclear transition metal complexes in Si- or Ge-sesquioxane frameworks: A review. *J. Organomet. Chem.* **2017**, *849–850*, 201–218. [[CrossRef](#)]
73. Quadrelli, E.A.; Basset, J.-M. On silsesquioxanes' accuracy as molecular models for silica-grafted complexes in heterogeneous catalysis. *Coord. Chem. Rev.* **2010**, *254*, 707–728. [[CrossRef](#)]
74. Levitsky, M.M.; Bilyachenko, A.N.; Shubina, E.S.; Long, J.; Guari, Y.; Larionova, J. Magnetic cage-like metallasilsesquioxanes. *Coord. Chem. Rev.* **2019**, *398*, 213015. [[CrossRef](#)]



75. Bilyachenko, A.N.; Yalymov, A.; Dronova, M.; Korlyukov, A.A.; Vologzhanina, A.V.; Es'Kova, M.A.; Long, J.; Larionova, J.; Guari, Y.; Dorovatovskii, P.V.; et al. Family of Polynuclear Nickel Cage-like Phenylsilsesquioxanes; Features of Periodic Networks and Magnetic Properties. *Inorg. Chem.* **2017**, *56*, 12751–12763. [[CrossRef](#)]
76. Liu, Y.-N.; Hou, J.-L.; Wang, Z.; Gupta, R.K.; Jagličić, Z.; Jagodič, M.; Wang, W.-G.; Tung, C.-H.; Sun, D. An Octanuclear Cobalt Cluster Protected by Macrocyclic Ligand: In Situ Ligand-Transformation-Assisted Assembly and Single-Molecule Magnet Behavior. *Inorg. Chem.* **2020**, *59*, 5683–5693. [[CrossRef](#)] [[PubMed](#)]
77. Bilyachenko, A.N.; Levitsky, M.M.; Yalymov, A.I.; Korlyukov, A.A.; Vologzhanina, A.V.; Kozlov, Y.N.; Shul'Pina, L.S.; Nesterov, D.S.; Pompeiro, A.J.L.; Lamaty, F.; et al. A heterometallic (Fe<sub>6</sub>Na<sub>8</sub>) cage-like silsesquioxane: Synthesis, structure, spin glass behavior and high catalytic activity. *RSC Adv.* **2016**, *6*, 48165–48180. [[CrossRef](#)]
78. Bilyachenko, A.N.; Levitsky, M.M.; Yalymov, A.I.; Korlyukov, A.A.; Khrustalev, V.N.; Vologzhanina, A.V.; Shul'Pina, L.S.; Ikonnikov, N.S.; Trigub, A.E.; Dorovatovskii, P.V.; et al. Cage-like Fe<sub>6</sub>Na-Germesquioxanes: Structure, Magnetism, and Catalytic Activity. *Angew. Chem. Int. Ed.* **2016**, *55*, 15360–15363. [[CrossRef](#)] [[PubMed](#)]
79. Bilyachenko, A.N.; Yalymov, A.I.; Korlyukov, A.A.; Long, J.; Larionova, J.; Guari, Y.; Vologzhanina, A.V.; Es'Kova, M.A.; Shubina, E.S.; Levitsky, M.M. Unusual penta- and hexanuclear Ni(II)-based silsesquioxane polynuclear complexes. *Dalton Trans.* **2016**, *45*, 7320–7327. [[CrossRef](#)] [[PubMed](#)]
80. Liu, L.; Lu, H.; Wang, H.; Bei, Y.; Feng, S. Luminescent organo-polysiloxanes containing complexed lanthanide ions. *Appl. Organomet. Chem.* **2009**, *23*, 429–433. [[CrossRef](#)]
81. Balzani, V.; Ceroni, P.; Juris, A. *Photochemistry and Photophysics: Concepts, Research, Applications*; John Wiley & Sons: Hoboken, NJ, USA, 2014; ISBN 978-3-527-67104-5.
82. Leonard, J.P.; Nolan, C.B.; Stomeo, F.; Gunnlaugsson, T. Photochemistry and Photophysics of Coordination Compounds: Lanthanides. In *Photochemistry and Photophysics of Coordination Compounds II*; Balzani, V., Campagna, S., Eds.; Topics in Current Chemistry; Springer: Berlin/Heidelberg, Germany, 2007; pp. 1–43. ISBN 978-3-540-73349-2.
83. Ning, Y.; Zhu, M.; Zhang, J.-L. Near-infrared (NIR) lanthanide molecular probes for bioimaging and biosensing. *Coord. Chem. Rev.* **2019**, *399*, 213028. [[CrossRef](#)]
84. Wahsner, J.; Gale, E.M.; Rodríguez-Rodríguez, A.; Caravan, P. Chemistry of MRI Contrast Agents: Current Challenges and New Frontiers. *Chem. Rev.* **2019**, *119*, 957–1057. [[CrossRef](#)]
85. Carniato, F.; Tei, L.; Botta, M. Gd-Based Mesoporous Silica Nanoparticles as MRI Probes. *Eur. J. Inorg. Chem.* **2018**, *2018*, 4936–4954. [[CrossRef](#)]
86. Amoroso, A.J.; Pope, S.J.A. Using lanthanide ions in molecular bioimaging. *Chem. Soc. Rev.* **2015**, *44*, 4723–4742. [[CrossRef](#)]
87. Hasegawa, Y.; Kitagawa, Y. Thermo-sensitive luminescence of lanthanide complexes, clusters, coordination polymers and metal-organic frameworks with organic photosensitizers. *J. Mater. Chem. C* **2019**, *7*, 7494–7511. [[CrossRef](#)]
88. Brites, C.D.S.; Millán, A.; Carlos, L.D. Chapter 281—Lanthanides in Luminescent Thermometry. In *Handbook on the Physics and Chemistry of Rare Earths*; Jean-Claude, B., Vitalij, K.P., Eds.; Including Actinides; Elsevier: Amsterdam, The Netherlands, 2016; Volume 49, pp. 339–427.
89. Bünzli, J.-C.G. On the design of highly luminescent lanthanide complexes. *Coord. Chem. Rev.* **2015**, *293–294*, 19–47. [[CrossRef](#)]
90. Andres, J.; Chauvin, A.-S. Colorimetry of Luminescent Lanthanide Complexes. *Molecules* **2020**, *25*, 4022. [[CrossRef](#)]
91. Armelao, L.; Quici, S.; Barigelletti, F.; Accorsi, G.; Bottaro, G.; Cavazzini, M.; Tondello, E. Design of luminescent lanthanide complexes: From molecules to highly efficient photo-emitting materials. *Coord. Chem. Rev.* **2010**, *254*, 487–505. [[CrossRef](#)]
92. Cui, Y.; Chen, B.; Qian, G. Lanthanide metal-organic frameworks for luminescent sensing and light-emitting applications. *Coord. Chem. Rev.* **2014**, *273–274*, 76–86. [[CrossRef](#)]
93. Zucchi, C.; Shchegolikhina, O.; Borsari, M.; Cornia, A.; Gavioli, G.; Fabretti, A.; Rentschler, E.; Gatteschi, D.; Ugo, R.; Psaro, R.; et al. Cyclooligosiloxanolate cluster complexes of transition metals and lanthanides. *J. Mol. Catal. A Chem.* **1996**, *107*, 313–321. [[CrossRef](#)]
94. Shchegolikhina, O.; Pozdniakova, Y.; Lindeman, S.; Zhdanov, A.; Psaro, R.; Ugo, R.; Gavioli, G.; Battistuzzi, R.; Borsari, M.; Rüffer, T.; et al. Cyclosiloxane sandwich complexes of a lanthanide metal: Na<sub>6</sub>[(C<sub>6</sub>H<sub>5</sub>SiO<sub>2</sub>)<sub>8</sub>]<sub>2</sub>Nd<sub>4</sub>(μ<sub>4</sub>-O)}. *J. Organomet. Chem.* **1996**, *514*, 29–35. [[CrossRef](#)]
95. Igonin, V.A.; Lindeman, S.V.; Struchkov, Y.T.; Molodtsova, Y.A.; Pozdnyakova, Y.A.; Shchegolikhina, O.I.; Zhdanov, A.A. Crystal structure of the Nd, Gd, and Dy sandwich complexes involving 8-membered macrocyclic phenylsiloxanolate ligands. *Russ. Chem. Bull.* **1993**, *42*, 176–181. [[CrossRef](#)]
96. Igonin, V.A.; Lindeman, S.V.; Struchkov, Y.T.; Shchegolikhina, O.I.; Molodtsova, Y.A.; Pozdnyakova, Y.A.; Zhdanov, A.A. Crystal structure of the La<sup>3+</sup> sandwich complex based on 8-membered macrocyclic siloxanolate ligands. *Russ. Chem. Bull.* **1993**, *42*, 168–173. [[CrossRef](#)]
97. Kulakova, A.N.; Bilyachenko, A.N.; Levitsky, M.M.; Khrustalev, V.N.; Shubina, E.S.; Felix, G.; Mamontova, E.; Long, J.; Guari, Y.; Larionova, J. New Luminescent Tetranuclear Lanthanide-Based Silsesquioxane Cage-Like Architectures. *Chem. A Eur. J.* **2020**, *26*, 16594–16598. [[CrossRef](#)]
98. Kaczmarek, A.M.; Esquivel, D.; LaForce, B.; Vincze, L.; Van Der Voort, P.; Romero-Salguero, F.J.; Van Deun, R. Luminescent thermometer based on Eu<sup>3+</sup>/Tb<sup>3+</sup>-organic-functionalized mesoporous silica. *Luminescence* **2018**, *33*, 567–573. [[CrossRef](#)]

99. Kulakova, A.N.; Nigoghossian, K.; Félix, G.; Khrustalev, V.N.; Shubina, E.S.; Long, J.; Guari, Y.; Carlos, L.D.; Bilyachenko, A.N.; Larionova, J. New Magnetic and Luminescent Dy(III) and Dy(III)/Y(III) Based Tetranuclear Silsesquioxane Cages. *Eur. J. Inorg. Chem.* **2021**, *2021*, 2696–2701. [[CrossRef](#)]
100. Shi, Y.; Gao, X.; Zhang, D.; Liu, Y.; Huang, G. Synthesis and thermal properties of modified room temperature vulcanized (RTV) silicone rubber using polyhedral oligomeric silsesquioxane (POSS) as a cross linking agent. *RSC Adv.* **2014**, *4*, 41453–41460. [[CrossRef](#)]
101. Dudzic, B.; Marciniak, B. Double-decker Silsesquioxanes: Current Chemistry and Applications. *Curr. Org. Chem.* **2018**, *21*. [[CrossRef](#)]
102. Duszczak, J.; Mituła, K.; Santiago-Portillo, A.; Soumoy, L.; Rzonsowska, M.; Januszewski, R.; Fusaro, L.; Aprile, C.; Dudzic, B. Double-Decker Silsesquioxanes Self-Assembled in One-Dimensional Coordination Polymeric Nanofibers with Emission Properties. *ACS Appl. Mater. Interfaces* **2021**, *13*, 22806–22818. [[CrossRef](#)]
103. Tanaka, T.; Hasegawa, Y.; Kawamori, T.; Kunthom, R.; Takeda, N.; Unno, M. Synthesis of Double-Decker Silsesquioxanes from Substituted Difluorosilane. *Organometallics* **2019**, *38*, 743–747. [[CrossRef](#)]
104. Barry, B.-D.; Dannatt, J.E.; King, A.K.; Lee, A.; Maleczka, R.E. A general diversity oriented synthesis of asymmetric double-decker shaped silsesquioxanes. *Chem. Commun.* **2019**, *55*, 8623–8626. [[CrossRef](#)] [[PubMed](#)]
105. Kunthom, R.; Takeda, N.; Unno, M. Synthesis and Characterization of Unsymmetrical Double-Decker Siloxane (Basket Cage). *Molecules* **2019**, *24*, 4252. [[CrossRef](#)]
106. Smith, B.C. *Infrared Spectral Interpretation: A Systematic Approach*; CRC Press: Boca Raton, FL, USA, 1999; ISBN 978-0-8493-2463-5.
107. Carniato, F.; Boccaleri, E.; Marchese, L.; Fina, A.; Tabuani, D.; Camino, G. Synthesis and Characterisation of Metal Isobutyl-silsesquioxanes and Their Role as Inorganic–Organic Nanoadditives for Enhancing Polymer Thermal Stability. *Eur. J. Inorg. Chem.* **2007**, *2007*, 585–591. [[CrossRef](#)]
108. Cotton, S. *Lanthanide and Actinide Chemistry*; John Wiley & Sons: Hoboken, NJ, USA, 2013; ISBN 978-1-118-68136-7.
109. Li, Q.; Li, T.; Wu, J. Luminescence of Europium(III) and Terbium(III) Complexes Incorporated in Poly(Vinyl Pyrrolidone) Matrix. *J. Phys. Chem. B* **2001**, *105*, 12293–12296. [[CrossRef](#)]
110. Marchesi, S.; Bisio, C.; Carniato, F. Novel light-emitting clays with structural Tb<sup>3+</sup> and Eu<sup>3+</sup> for chromate anion detection. *RSC Adv.* **2020**, *10*, 29765–29771. [[CrossRef](#)]
111. Binnemans, K. Interpretation of europium(III) spectra. *Coord. Chem. Rev.* **2015**, *295*, 1–45. [[CrossRef](#)]
112. Carrasco, I.; Piccinelli, F.; Bettinelli, M. Luminescence of Tb-based materials doped with Eu<sup>3+</sup>: Case studies for energy transfer processes. *J. Lumin.* **2017**, *189*, 71–77. [[CrossRef](#)]
113. Rodrigues, M.O.; Dutra, J.D.L.; Nunes, L.A.O.; de Sá, G.F.; de Azevedo, W.M.; Silva, P.; Paz, F.A.A.; Freire, R.O.; Júnior, S.A. Tb<sub>3+</sub> → Eu<sub>3+</sub> Energy Transfer in Mixed-Lanthanide–Organic Frameworks. *J. Phys. Chem. C* **2012**, *116*, 19951–19957. [[CrossRef](#)]
114. Hou, Z.; Cheng, Z.; Li, G.; Wang, W.; Peng, C.; Li, C.; Ma, P.; Yang, D.; Kang, X.; Lin, J. Electrospinning-derived Tb<sub>2</sub>(WO<sub>4</sub>)<sub>3</sub>:Eu<sup>3+</sup> nanowires: Energy transfer and tunable luminescence properties. *Nanoscale* **2011**, *3*, 1568–1574. [[CrossRef](#)] [[PubMed](#)]
115. Binnemans, K.; Görlner-Walrand, C. Application of the Eu<sup>3+</sup> Ion for Site Symmetry Determination. *J. Rare Earth* **1996**, *14*, 173–180.
116. Tang, S.; Babai, A.; Mudring, A.-V. Europium-Based Ionic Liquids as Luminescent Soft Materials. *Angew. Chem. Int. Ed.* **2008**, *47*, 7631–7634. [[CrossRef](#)]
117. Zhang, P.; Wang, Y.; Liu, H.; Chen, Y. Preparation and luminescence of europium(III) terpyridine complex-bridged polysilsesquioxanes. *J. Mater. Chem.* **2011**, *21*, 18462–18466. [[CrossRef](#)]
118. Yin, H.; Li, Y.; Bai, J.; Ma, M.; Liu, J. Effect of calcinations temperature on the luminescence intensity and fluorescent lifetime of Tb<sup>3+</sup>-doped hydroxyapatite (Tb-HA) nanocrystallines. *J. Materiomics* **2017**, *3*, 144–149. [[CrossRef](#)]
119. Sahu, I.P.; Bisen, D.; Tamrakar, R.K.; Murthy, K.; Mohapatra, M. Luminescence studies on the europium doped strontium metasilicate phosphor prepared by solid state reaction method. *J. Sci. Adv. Mater. Devices* **2017**, *2*, 59–68. [[CrossRef](#)]
120. Parker, D. Luminescent lanthanide sensors for pH, pO<sub>2</sub> and selected anions. *Coord. Chem. Rev.* **2000**, *205*, 109–130. [[CrossRef](#)]
121. Okamoto, S.; Vyprachticky, D.; Furuya, H.; Abe, A.; Okamoto, Y. Ion Binding Properties of Polycarboxylates Using Terbium(III) as a Fluorescent Probe: Viscosities and Coordinated Water Molecules in Polycarboxylate–Terbium(III) Complexes in Aqueous Solutions. *Macromolecules* **1996**, *29*, 3511–3514. [[CrossRef](#)]
122. Beeby, A.; Clarkson, I.M.; Dickins, R.S.; Faulkner, S.; Parker, D.; Royle, L.; de Sousa, A.S.; Williams, J.A.G.; Woods, M. Non-radiative deactivation of the excited states of europium, terbium and ytterbium complexes by proximate energy-matched OH, NH and CH oscillators: An improved luminescence method for establishing solution hydration states. *J. Chem. Soc. Perkin Trans.* **1999**, *2*, 493–504. [[CrossRef](#)]
123. Supkowski, R.M.; Horrocks, W.D. On the determination of the number of water molecules, q, coordinated to europium(III) ions in solution from luminescence decay lifetimes. *Inorg. Chim. Acta* **2002**, *340*, 44–48. [[CrossRef](#)]
124. Cotton, S.A. Scandium, Yttrium & the Lanthanides: Inorganic & Coordination Chemistry. In *Encyclopedia of Inorganic and Bioinorganic Chemistry*; Scott, R.A., Ed.; John Wiley & Sons, Ltd: Chichester, UK, 2011; p. eibc0195. ISBN 978-1-119-95143-8.
125. Olivero, F.; Carniato, F.; Bisio, C.; Marchese, L. Promotion of Förster Resonance Energy Transfer in a Saponite Clay Containing Luminescent Polyhedral Oligomeric Silsesquioxane and Rhodamine Dye. *Chem. Asian J.* **2014**, *9*, 158–165. [[CrossRef](#)] [[PubMed](#)]



126. Cucinotta, F.; Carniato, F.; Devaux, A.; De Cola, L.; Marchese, L. Efficient Photoinduced Energy Transfer in a Newly Developed Hybrid SBA-15 Photonic Antenna. *Chem. A Eur. J.* **2012**, *18*, 15310–15315. [[CrossRef](#)] [[PubMed](#)]
127. Xie, J.; Cheng, L.; Tang, H.; Wang, Z.; Sun, H.; Lu, L.; Mi, X.; Liu, Q.; Zhang, X. Wide range color tunability and efficient energy transfer of novel NaCaGd(WO<sub>4</sub>)<sub>3</sub>:Tb<sup>3+</sup>·Eu<sup>3+</sup> phosphors with excellent thermal stability for pc-WLEDs. *Inorg. Chem. Front.* **2021**, *8*, 4517–4527. [[CrossRef](#)]